AGU PUBLICATIONS

JGR

Journal of Geophysical Research: Space Physics

RESEARCH ARTICLE
10.1002/2016JA022847

A sequence of flux transfer events potentially generated by different generation mechanisms

L. Trenchi[1], R. C. Fear[1], K. J. Trattner[2], B. Mihaljcic[3], and A. N. Fazakerley[3]

[1]Department of Physics and Astronomy, University of Southampton, Southampton, UK, [2]LASP, University of Colorado Boulder, Boulder, Colorado, USA, [3]Mullard Space Science Laboratory, UCL, Dorking, UK

Key Points:
- Reconnection jets are systematically associated with the trailing edge of these FTEs; this suggests the single X line generation mechanism
- The FTEs observed during this event are potentially generated by different generation mechanisms: single X line and multiple X lines
- The asymmetric Bn signature observed during one FTE is probably explained by an outward motion of the magnetopause

Supporting Information:
- Supporting Information S1

Correspondence to:
L. Trenchi,
L.Trenchi@soton.ac.uk

Citation:
Trenchi, L., R. C. Fear, K. J. Trattner, B. Mihaljcic, and A. N. Fazakerley (2016), A sequence of flux transfer events potentially generated by different generation mechanisms, *J. Geophys. Res. Space Physics*, *121*, 8624–8639, doi:10.1002/2016JA022847.

Received 21 APR 2016
Accepted 18 AUG 2016
Accepted article online 22 AUG 2016
Published online 23 SEP 2016

Abstract Flux transfer events (FTEs) are magnetic structures generated by time-varying reconnection at the dayside magnetopause. Understanding their generation mechanism is important, because it is necessary in order to understand the global contribution of FTEs to the convection process. We present observations of several FTEs sequentially observed by Cluster at the subsolar magnetopause. Cluster detected also several reconnection jets, which seem to be systematically associated with the trailing edge of the FTEs. This association is expected only in the FTEs formed by single X line reconnection but could be compatible also with the multiple X line model, when reconnection at one X line is dominant. Instead, it does not seem compatible with original mechanism proposed by Russell and Elphic (1978). For a large FTE, not associated with any reconnection jet, the Grad-Shafranov reconstruction obtained from Cluster 1 data recovers a flux rope, indicative of multiple X line reconnection. This same FTE was detected also by Cluster 3, which observed an asymmetric signature in the magnetic field component normal to the magnetopause. We show that this asymmetric signature was caused by an outward motion of the magnetopause. The orientation of the other FTEs, obtained from a Grad-Shafranov optimization, shows considerable spread, despite the relatively steady conditions. Our interpretation is that a combination of single and multiple X line reconnection generated these FTEs. The FTEs in the first part of the crossing, associated with reconnection jets, are generated by the single X line model and may therefore not satisfy the Grad-Shafranov assumptions so well. Instead, the last FTE, slower, bigger, and well separated from the previous ones, may be formed by multiple X line reconnection.

1. Introduction

Russell and Elphic [1978] were the first to use the term flux transfer event (FTE) to describe the rapid bipolar oscillations in the component of the magnetic field perpendicular to the magnetopause (B_N), which are often observed in proximity of the dayside magnetopause. These authors interpreted these bipolar signatures as the result of time-varying reconnection at the magnetopause.

Similar B_N signatures could also be due to the deformation of the magnetopause caused by solar wind pressure pulses or surface waves traveling along the magnetopause surface [*Lemaire et al.*, 1979; *Sibeck et al.*, 1989; *Sanny et al.*, 1996]. However, since the plasma inside the FTEs consists of a mixture of magnetosheath and magnetospheric plasmas [*Daly et al.*, 1981], there is a general consensus that these FTEs are a reconnection-related phenomenon [*Lockwood and Hapgood*, 1998]. Nevertheless, the generation mechanism of FTEs remains unclear, and therefore, several different models have been proposed.

In the original *Russell and Elphic* [1978] model, FTEs are elbow-shaped flux tubes of reconnected field lines generated by a burst of reconnection along a localized reconnection site, while the rest of the magnetopause remains a closed boundary. *Sonnerup* [1987] pointed out that in the *Russell and Elphic* [1978] model, the interaction of the FTE with the magnetic field lines inside the magnetopause generates induced currents, which in turn produce the twist of the field lines inside the FTEs. In this model, the bipolar B_N signature outside the FTE is related to the draping of the magnetosheath and magnetospheric field lines around the FTE, while inside the FTE the B_N signature is due to the helical topology of the FTE field lines (a flux rope topology).

Lee and Fu [1985] related instead FTEs to the presence of multiple X lines at the magnetopause. In this model, the simultaneous reconnection along multiple extended X lines generates FTEs that are elongated helical magnetic flux ropes with the axis roughly aligned with the X lines. The formation of the multiple X lines could

be due to the tearing instability at the magnetopause [*Lee and Fu*, 1985] or, alternatively, to a large inclination of the Earth's magnetic dipole due to seasonal effects [*Raeder*, 2006].

Alternatively, *Scholer* [1988] and *Southwood et al.* [1988] proposed that the FTEs are due to a burst of reconnection along a single but extended X line. In this case, the FTE consists of a bulge of hot plasma accelerated abruptly by the reconnection burst and heated by two propagating shock waves [*Biernat et al.*, 1987]. The increased thermal pressure of this hot plasma produces a bubble-like structure of reconnected field lines that propagates away from the X line. Also, in this model the FTE is a two-dimensional structure with the axis roughly aligned with the X line. In this case, however, the FTE is not a flux rope.

Studying how FTEs are generated is relevant because it helps to understand how magnetic reconnection occurs at the dayside magnetopause. Moreover, which of these models occurs affects also the amount of magnetic flux that is opened by each FTE [*Fear et al.*, 2008]. All these different FTE models predict the same characteristic bipolar B_N signature observed at the magnetopause; however, the predictions are quite different for the overall FTE geometry, motion, and field topology. Therefore, detailed analysis of plasma and magnetic field data measured by the spacecraft during the FTEs can give useful indications about their generation mechanism.

For example, when the magnetic shear angle is large, the orientation of the FTE axis and the scale size of the FTEs along the magnetopause are critical parameters to understand the FTE generation mechanism. In both the single and multiple X line models the FTEs are expected to have an extended magnetopause section with the axis roughly parallel to the X line direction and therefore should be structures more elongated along the azimuthal direction. In contrast, in the Russell and Elphic model, the FTE axis should be along the magnetosheath or magnetospheric fields, i.e., along the north-south direction, and therefore, the FTE latitudinal scale should be larger than its azimuthal scale.

Several studies reported FTEs with the axis approximately aligned with the X line direction, which are more in agreement with the extended (single or multiple) X line models [*Trenchi et al.*, 2011; *Fear et al.*, 2012]. Consistent with this interpretation, FTE scale sizes obtained from multispacecraft studies are sometimes found to be more extended along the azimuthal extent [*Fear et al.*, 2008], but on the other hand, some studies report events that are more extended along the poleward direction [*Kawano and Russell*, 2005].

The detailed analysis of the characteristics of the plasma inside the FTEs can help to distinguish among the various generation mechanisms [*Lockwood and Hapgood*, 1998; *Varsani et al.*, 2014]. Moreover, also the relation of the FTEs with reconnection jets can give important indications to understand the origin of the FTEs. Several studies reported FTEs bounded by two converging reconnection jets and interpreted these as the evidence of multiple X line generation mechanism [*Hasegawa et al.*, 2010; *Trenchi et al.*, 2011; *Øieroset et al.*, 2011; *Zhang et al.*, 2012; *Zhong et al.*, 2013; *Pu et al.*, 2013].

Another complementary approach consists of the analysis of the magnetic field topology of the FTEs by adopting the Grad-Shafranov reconstruction technique. This method produces magnetic field maps that give a direct visualization of the magnetic field configuration in extended regions near the spacecraft. Several studies based on the Grad-Shafranov method have reported FTEs that are magnetic flux ropes characterized by strong axial fields, suggesting a multiple X line generation mechanism [*Sonnerup et al.*, 2004; *Hasegawa et al.*, 2006, 2010].

In this paper, we present the detailed analysis of several FTEs sequentially observed by Cluster spacecraft during the magnetopause crossing observed on 27 March 2007. This particular interval has previously been studied by *Fear et al.* [2010, 2012] but has two major features which make it attractive for further study in order to investigate the differences between formation mechanisms: the magnetic shear angle was very large and the interspacecraft separation was approximately 9000 km. In this paper, we examine the relative position of the reconnection jets with respect to these FTEs, and we determine the orientation of these FTEs from the Grad-Shafranov analysis and from multispacecraft analysis. We also perform Grad-Shafranov reconstruction to recover the magnetic field topology of a large FTE. The results of these analyses are discussed in the framework of the main FTE models cited above.

2. Event Overview

Figure 1 displays the plasma and magnetic field data measured by Cluster 1 on 27 March 2007 during the magnetopause crossing which occurred near the subsolar point at $(9.2, -1.3, 2.8)_{GSM}$ R_E. Figure 1

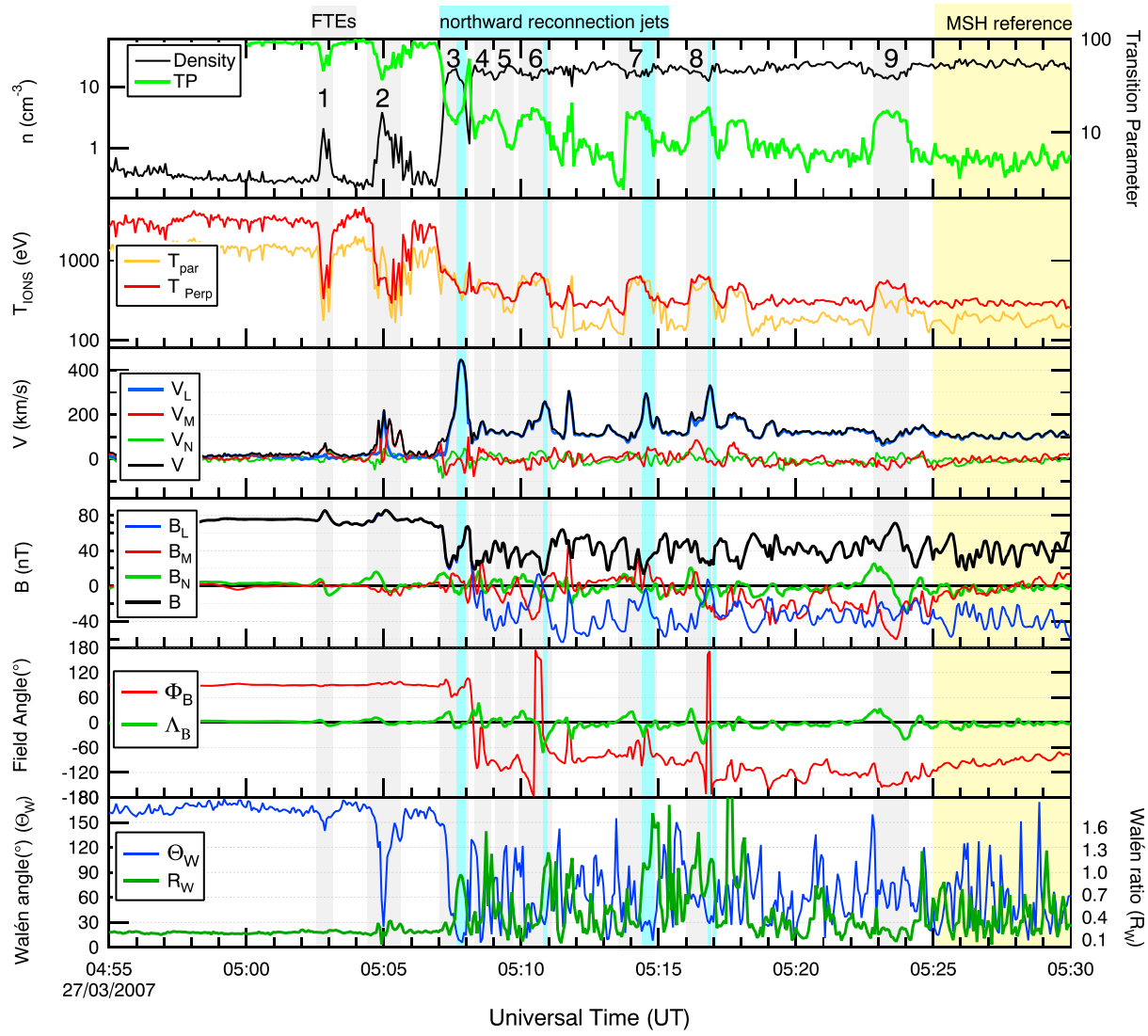

Figure 1. Magnetopause crossing observed by Cluster 1, on 27 March 2007. Displayed are the (first panel) plasma density, (second panel) temperatures, and (third panel) velocity vector measured by HIA. (fourth panel) The components and (fifth panel) the two polar angles of the magnetic field vector. The velocity and magnetic field vectors are displayed in the *LMN* reference frame. Figure 1 (first panel) shows the transition parameter, while Figure 1 (fifth panel) shows the two parameters used to evaluate the agreement of the Walén test.

(first to third panels) shows the ion density, temperatures, and velocity vector measured by the Hot Ion Analyzer (HIA) [*Rème et al.*, 2001], while Figure 1 (fourth panel) displayed the magnetic field components measured by the fluxgate magnetometer (FGM) instrument [*Balogh et al.*, 1207]. For the velocity and magnetic field vector, we used here the same local boundary normal reference frame (*LMN*) [*Russell and Elphic*, 1978] determined by *Fear et al.* [2012] from the minimum variance analysis: the *N* direction is outward along the local magnetopause normal, while *L* and*M* are in the plane defined by *N*, being northward and dawnward, respectively. The magnetic field orientation is also displayed in Figure 1 (fifth panel) using the two polar angles defined as Φ_B=$\tan^{-1}\left(B_L/B_M\right)$, $\Lambda_B = \tan^{-1}\left(B_N/\left(B_L^2+B_M^2\right)^{0.5}\right)$ in the range [−180°, +180°] and [−90°, +90°], respectively.

Before 5:08 UT Cluster 1 was located in the magnetosphere, where it detected magnetospheric plasma characterized by low density ($n<1$ (cm^{-3})) and high temperature ($T\sim2000$ eV) and the magnetic field was along positive *L*. A complete outbound magnetopause crossing into the magnetosheath was observed around 05:08 UT, when the B_L component became negative and the plasma density increased above 10 cm^{-3}. Moreover, Cluster 1 observed several other encounters with the magnetopause boundary layer, where the

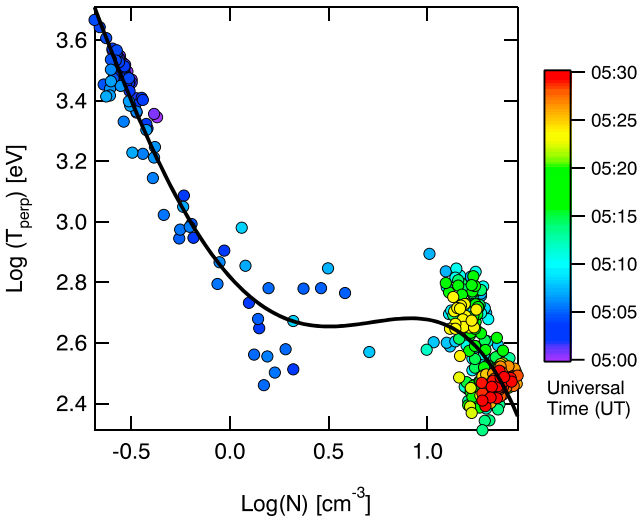

Figure 2. The ion-perpendicular temperatures as a function of the ion densities measured by Cluster 1 in the time interval 05:00–05:30 UT (the time of each measurement is shown with the color scale) in a log-log scale. The black line is the fourth-order polynomial best fit. Each data point is projected into the nearest point along the fitting curve, and the transition parameter is obtained from the distance along this curve, normalizing the magnetosheath extreme (bottom right end) as 0 and the magnetospheric extreme (top left end) as 100.

plasma temperatures and density assume an intermediate value between magnetosheath and magnetospheric values.

The magnetosheath magnetic field was characterized by several fluctuations on time scales of approximately 1 min. While these fluctuations are evident in the individual magnetic field components, they involve mainly the magnetic field intensity while the magnetic field orientation remains quite stable (see the polar angles in Figure 1 (fifth panel)). In addition, the plasma pressure exhibits fluctuations on similar time scales that are generally anticorrelated with the fluctuation of the magnetic field magnitude, such that the local pressure equilibrium is approximately maintained (not shown). *Laitinen et al.* [2010] studied this interval and classified these fluctuations as due to mirror mode structures.

The B_N magnetic field component and consequently Λ_B are nearly zero on average, but they exhibit several positive-negative bipolar perturbations, both before and after the MP crossing, which are typical signatures of flux transfer events (FTEs) with standard polarity. The grey shadings highlight some of the more clear FTEs observed during this interval. In particular, the FTE numbers 1–9 are taken from the "core crossing" events C1–C9 identified by *Fear et al.* [2012] for Cluster 1.

3. The Transition Parameter

An estimation of the relative position of Cluster 1 with respect to the magnetopause as a function of time can be obtained from the value of transition parameter, which is based on plasma density and temperature measured at the magnetopause or in the boundary layer [*Hapgood and Bryant*, 1990, 1992; *Fear et al.*, 2005; *Bogdanova et al.*, 2008]. Indeed, according to the model of *Lockwood et al.* [1996], the mixing of the magnetosheath and magnetospheric populations in the boundary layer is related to time of flight effects in the reconnection layer. In particular, the magnetosheath and magnetospheric populations experience a velocity cutoff at the two rotational discontinuities emanating from the reconnection site [*Petschek*, 1964]. The value of the velocity cutoff changes gradually inside the reconnection layer, and it becomes infinite at the separatrix. Therefore, the value of the transition parameter can be considered as a measure of the penetration of the spacecraft into the boundary layer [*Lockwood and Hapgood*, 1997].

In the scatterplot in Figure 2, we display on a log-log scale the ion-perpendicular temperatures as a function of the ion densities measured by Cluster 1 in the time interval 05:00–05:30 UT (the time of each measurement is shown by the color scale), and the black line is the fourth-order polynomial best fit. The magnetosheath proper is located in the bottom right corner of this graph, characterized by low temperature and high density, while the measurements in the magnetosphere are located in the top left corner, where the plasma temperature is high and the density is low.

The points in central part of this graph refer instead to the boundary layer. Often, it is found that two sublayers with different properties form the boundary layer: an outer boundary layer, similar to the magnetosheath population but with lower density, and the inner boundary layer, more similar to the magnetospheric population, where a gradual variation of the temperature is observed [*Song et al.*, 1990]. Here instead, we have several measurements in the inner boundary layer ($\mathrm{Log}(N) < 0.5$ cm^{-3}) but very few in the outer boundary layer. This feature is consistent with the thin boundary layer expected when the interplanetary magnetic field is southward [*Mitchell et al.*, 1987; *Němeček et al.*, 2015], as it is during this magnetopause crossing.

We note in passing that the transition parameter is usually calculated from electron densities and temperatures. For this interval event, the transition parameter based on electron data (not shown) shows a similar trend to the transition parameter based on ion. However, it has a lower sensitivity during the magnetosheath interval and hence the variations through FTEs 6 to 8 are not as clearly drawn out. For this reason we used the transition parameter based on ion data.

Each data point in this figure is projected onto the nearest point along the fitted curve. The transition parameter (TP) is defined as the distance of the projected points along this curve, normalized to the extrema, defined as 0 in the magnetosheath side and 100 in the magnetospheric side. The values of the TP are reported in Figure 1 (first panel) (right-hand axis).

Before the magnetopause crossing, the TP was large and stable, except for the two small decreases observed during the FTEs 1 and 2. The TP showed a substantial decrease at the magnetopause crossing, remaining smaller than 20 after 5:08 UT. TP was approximately 5 during the magnetosheath proper and ~15 during the encounters with the boundary layer. Most of these encounters with the boundary layer occurred in coincidence with the FTEs since the passage of the FTE structures produced a deformation of the magnetopause that caused the approach of the spacecraft with the magnetopause [*Hapgood and Lockwood*, 1995].

4. FTE Relation With Reconnection Jets

A key feature of this magnetopause crossing that has not previously been discussed is the relation between FTEs and the plasma jets observed by Cluster 1, characterized by enhanced velocity with respect to the adjacent magnetosheath along the positive L direction (e.g., at 5.08, 5.15, and 5.17 UT). In order to test if these jets are related to magnetic reconnection, we performed the Walén test in the spacecraft reference frame. This test is particularly useful since it allows an easy identification of the time intervals that satisfy the Walén relation (i.e., reconnection jets), and it has been successfully applied in several studies of magnetic reconnection at the magnetopause [*Paschmann et al.*, 1986; *Phan et al.*, 1996; *Trenchi et al.*, 2008]. For each data point in the data interval shown in Figure 1, we compared the observed velocity jump relative to a reference value in the magnetosheath $V - V_{\mathrm{MSH}}$ (the magnetosheath reference is highlighted in Figure 1 by the yellow shading) with the expected velocity jump $\Delta\mathbf{V}_{\mathrm{th}}$ predicted by the Walén relation:

$$\Delta\mathbf{V}_{\mathrm{th}} = \pm\left[\left(1-\alpha_{\mathrm{MSH}}\right)/\mu_0\rho_{\mathrm{MSH}}\right]^{1/2}\left[\mathbf{B}(1-\alpha)/\left(1-\alpha_{\mathrm{MSH}}\right)-\mathbf{B}_{\mathrm{MSH}}\right] \quad (1)$$

where $\alpha = \left(p_{\parallel}-p_{\perp}\right)\mu_0/B^2$ is the anisotropy factor calculated from the difference between the parallel and perpendicular pressures [*Hudson*, 1970]. Comparing these two vectors, we obtained the two parameters used to evaluate the agreement of the Walén relation: R_W as the ratio of their absolute values and Θ_W as their relative angle, displayed in Figure 1 (fifth panel). We considered here that the Walén relation is satisfied when $R_W > 0.4$ and $\Theta_W < 30°$ for observations northward of the reconnection X line, while it is satisfied when $R_W > 0.4$ and $\Theta_W > 150°$ for observations southward of the X line (more details in *Trenchi et al.* [2008]).

The light blue shadings in Figure 1 highlight the data intervals at the MP or in the boundary layer that satisfy the Walén relation, and that can be therefore considered as reconnection jets. All these reconnection jets satisfy the Walén relation with positive sign ($\Theta_W < 30°$), which means that Cluster is northward of the X line. This is consistent with the positive-negative polarity of the FTEs, which is expected for FTEs moving northward of the X line. Moreover, the X line location is probably stable during this event, since the X line motion due to the diamagnetic drift effect is negligible, given the small guide field resulting from the high magnetic shear angle [*Trenchi et al.*, 2015].

It can be noted that all these reconnection jets are observed during the second half of the FTEs 3 and 6–8, where the B_N component was negative. For these FTEs we performed also the Walén test in the de Hoffmann-Teller reference frame, including both the leading and the trailing edges, shown in the supporting information. During the FTEs 6–8, which are observed on the magnetosheath side of the magnetopause, the deepest penetration into the boundary layer is observed approximately at the center of the FTEs, where the TP reaches its maximum value. FTE 3 appears to be observed exactly as the spacecraft crosses the magnetopause, but careful examination of the TP shows that the TP increases back toward magnetospheric values on the trailing edge; therefore, this event is observed just on the magnetospheric side of the magnetopause. Therefore, for FTE 3, the maximum penetration into the boundary layer corresponds to the minimum value of TP, also in this case approximately at the center of the FTE. For all these FTEs, the reconnection jet is observed

after the maximum penetration into the boundary layer, when the TP has the same value as in the first half of these FTEs. This suggests that the detection of the reconnection jets is not related to the deepest penetration into the boundary layer, but instead, these reconnection jets are propagating at the trailing edge of the FTEs. This feature can give some important information about the FTE generation mechanism.

Indeed, these reconnection jets at the trailing edge of the FTEs suggest the single X line model [*Scholer*, 1988; *Southwood et al.*, 1988], which is the only FTE model that explicitly predicts a reconnection jet moving in the same direction of the FTE, propagating at his trailing edge [*Lockwood and Smith*, 1994]. In the other FTE models, the expected relation with reconnection jets is different.

In the original *Russell and Elphic* [1978] model, the magnetic tension of the elbow-shaped FTE field lines could cause a poleward acceleration of the plasma inside the FTE even if reconnection is not active at the time of FTE observation, i.e., if the FTE is no longer magnetically connected to the reconnection site. This poleward acceleration is expected only when the FTE size exceeds a certain critical dimension [*Sonnerup*, 1987]. In this model, however, the velocity increase should be observed throughout the entire FTE, and not only at its trailing edge.

In the multiple X line model [*Lee and Fu*, 1985], two converging reconnection jets at the borders of the FTE are expected when the FTE is observed during its formation [*Hasegawa et al.*, 2010; *Trenchi et al.*, 2011; *Øieroset et al.*, 2011; *Zhang et al.*, 2012; *Zhong et al.*, 2013; *Pu et al.*, 2013]. Therefore, for this model the discrepancy with respect to our observations is the lack of the southward reconnection jet at the leading edge of the FTEs. The lack of southward jets could be justified in the context of multiple X line reconnection, if reconnection at the northward reconnection line is not active when the FTEs are observed. In this case, in effect, a combination of both multiple X line model and single X line model contributes to the formation of the FTE, and the FTE would consist of a flux rope in the FTE center, generated when reconnection was active at both the X lines, and open field lines produced by single X line reconnection in the more external FTE region [see *Hasegawa et al.*, 2010, Figure 1c].

5. Grad-Shafranov Analysis

In order to further investigate the suggestion that single X line reconnection may play a key role in the formation of the flux transfer event signatures observed on this magnetopause crossing (possibly supported by multiple X line reconnection through a much less active secondary X line), we analyzed all these FTEs using the Grad-Shafranov (GS) reconstruction. This method can be applied to any plasma/magnetic field structures that are approximately in two-dimensional (2-D) MHD equilibrium and produces magnetic field maps that give a direct visualization of the magnetic field configuration in extended regions near the spacecraft [*Sonnerup et al.*, 2006]. This method, first developed by *Sonnerup and Guo* [1996] to study the structure of magnetopause current layer, has been successfully applied to a variety of coherent magnetohydrostatic structures observed in the solar wind [*Hu and Sonnerup*, 2001, 2002; *Hu et al.*, 2004] at the magnetopause [*Lui et al.*, 2008; *Hasegawa et al.*, 2010] and in the magnetotail [*Möstl et al.*, 2009].

One important part of the GS reconstruction consists of the determination of the invariant axis of the structure. For this purpose, it is very useful to use the optimization procedure based on the GS equation, which identifies the invariant axis (z) as the direction along which the transverse pressure P_t (defined as $P_t = \left(p_p + \frac{B_z^2}{2\mu_o}\right)$) is a single-value function of the z component of the vector potential A [*Hau and Sonnerup*, 1999; *Hu and Sonnerup*, 2002].

Fear et al. [2012] used one of these procedures to determine the orientation of the FTEs examined in the present study, assuming that the FTE axes are contained in the magnetopause plane [*Hau and Sonnerup*, 1999]. They performed this optimization using only the data measured in the FTE cores, where the characteristics of the electron distribution function suggested that the spacecraft was on open field lines, and they evaluated the correlation between P_t and A with the Spearman's rank correlation coefficient. With this approach, they obtained the orientations of all the nine FTEs, but they only considered four of the FTEs to have reliably determined axes (the FTEs 3, 5, 6, and 9 in Figure 1), because the other axial determinations were either based on a small number of data points or were characterized by a poor correlation between P_t and A.

However, strictly speaking, it is not necessary to restrict the GS analysis to the FTE core. For this reason we performed again this analysis, but in this case we used adaptive data intervals with the procedure described below, which allowed us to consider, for each FTE, more data points with respect to the previous analysis. We adopt here the procedure illustrated by *Hu and Sonnerup* [2002], which is also based on the requirement that

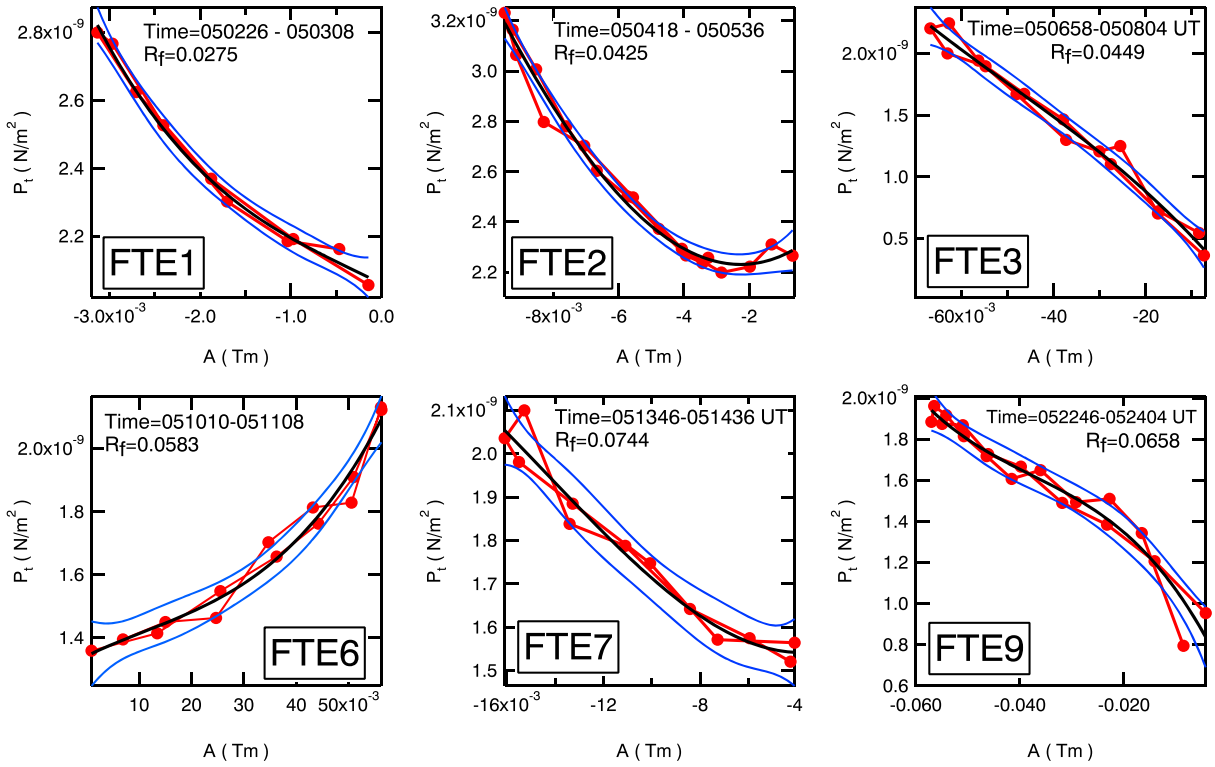

Figure 3. Each panel illustrates behavior of $P_t(A)$ (red lines) for the six FTEs for which we obtained reliable results from the Grad-Shafranov analysis. The black lines report the polynomial fits of $P_t(A)$ used for the GS analysis, and the blue lines represent the 95% confidence bands of the fit. These time intervals are selected from the optimization procedure, as the ones that show the lowest fitting residual R_f, i.e., the ones that better satisfy the GS assumptions.

the transverse pressure P_t is a function of the magnetic vector potential A alone, but it searches the invariant axis in the three-dimensional space. The deviation between P_t and A is obtained from the fits of $P_t(A)$ in the first and second parts of the signature (the entry into and exit from the FTE), using both second- and third-order polynomials (as illustrated by *Hu and Sonnerup*, 2002 [2002, Figure 1]), and as a comparison, we also evaluated the Spearman's rank correlation coefficient between P_t and A [*Fear et al.*, 2012].

For each FTE this optimization procedure is repeated several times, considering, each time, data intervals with different durations: we changed the starting times of the data interval analyzed by this optimization procedure every run, while the ending times are automatically determined by this procedure as described by *Hu and Sonnerup* [2002]. In this way, for each FTE we identified the data interval that best satisfies the GS assumptions, as the time interval that shows the lowest deviation between P_t and A (measured from the fitting residual R_f, using the same procedure as the one used in *Trenchi et al.* [2013]). This interval is chosen as the final data interval for the GS analysis (P_t versus A plots shown in Figure 3). We consider here that the results of this procedure are reliable and robust when (1) the orientations obtained by evaluating the correlations of $P_t(A)$ with the three methods described above (fits of $P_t(A)$ with second- and third-order polynomials and Spearman's rank correlation coefficient between P_t and A) are similar enough (deviations smaller than 10°–15°) and (2) the orientations remain stable using the data intervals of different duration.

With this procedure, we found reliable orientations for FTEs 1–3, 6, 7, and 9, which are shown in Figure 4 in the magnetopause *L-M* plane. It can be noted that the FTE orientations obtained from the GS analysis show considerable spread, even though the magnetosheath magnetic field orientation was stable during this time interval. With the exception of FTE 6, the orientation of each individual FTE agrees with the orientation determined by *Fear et al.* [2012] (see their Figure 11) to within 20°. However, the major difference between our results and those of *Fear et al.* [2012] lies in the determination of which axes are considered as reliable.

According to the GS analysis in this study, FTE 9 is the only FTE that has an axial orientation similar to the X line direction (which should be approximately along the *M* axis according to the component merging model [*Sonnerup*, 1974; *Gonzales and Mozer*, 1974] since the magnetosheath and magnetosphere

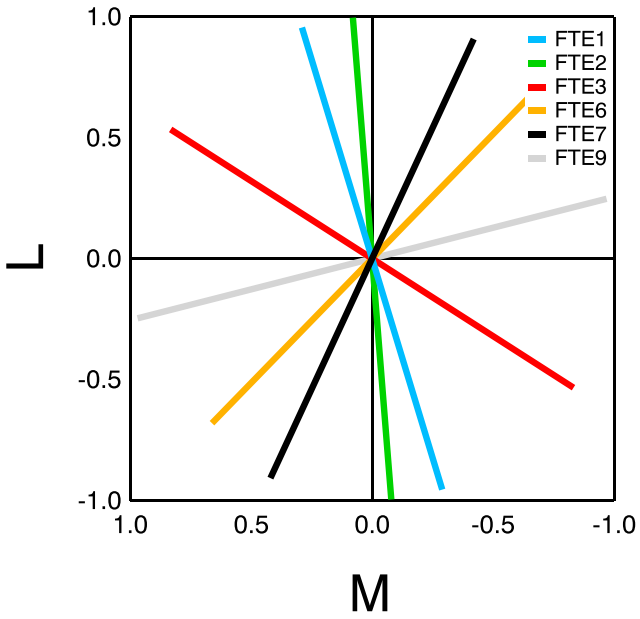

Figure 4. Orientations of the FTEs axis obtained from the Grad-Shafranov analysis in the magnetopause *L-M* plane.

fields are nearly antiparallel), while the orientations of the other FTEs (1–3, 6, and 7) differ substantially from the X line direction.

However, the choice of events determined to be reliable is not in agreement with *Fear et al.* [2012] who, according to their analysis, considered reliable only the FTE orientations oriented approximately along the dawn-dusk direction. The same orientation was also obtained from minimum variance analysis of "draping" FTE signatures observed earlier on the same crossing [*Fear et al.*, 2012]. Moreover, if Cluster 1 is observing a portion of the FTE where the curvature of the FTE structure is not negligible, the Grad-Shafranov technique would probably fail, because the two-dimensional approximation required by the GS equilibrium is violated. For this reason, in the next section we tried to evaluate the orientation of these FTEs from the multispacecraft analysis, examining the magnetic field data measured by the other Cluster spacecraft.

6. Orientation From Multispacecraft Analysis

Figure 5 shows the positions of the Cluster spacecraft relative to Cluster 3 during this magnetopause crossing, in *LMN* coordinates. In the *LM* plane, Cluster 1–3 are separated by 8500 km each other approximately, being at the vertices of an equilateral triangle, while Cluster 4 is quite close to Cluster 3. Conversely, their separation along *N* is much smaller (<1200 km). With this large separation, it is possible to determine the velocity and axial orientation of these FTEs from the multispacecraft timing, exploring the large-scale geometry of the FTEs. This analysis is based on the hypothesis that the axes of the FTE structures lie approximately in the magnetopause plane. The similarity between the magnetic field signatures detected by different spacecraft can be interpreted as a proof that the observed FTE structure has an axial extension larger than the spacecraft separation. With this respect, this method can be considered more reliable than the GS analysis. On the other hand, this method is based on the hypothesis that the similar magnetic signatures observed by the various

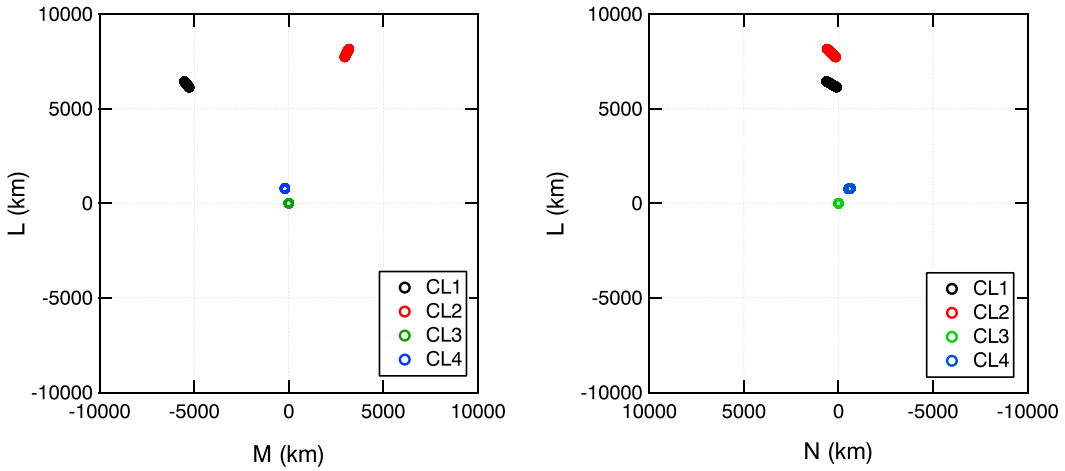

Figure 5. Relative positions of the Cluster spacecraft with respect to Cluster 3 position, in the (left) *L-M* and (right) *L-N*.

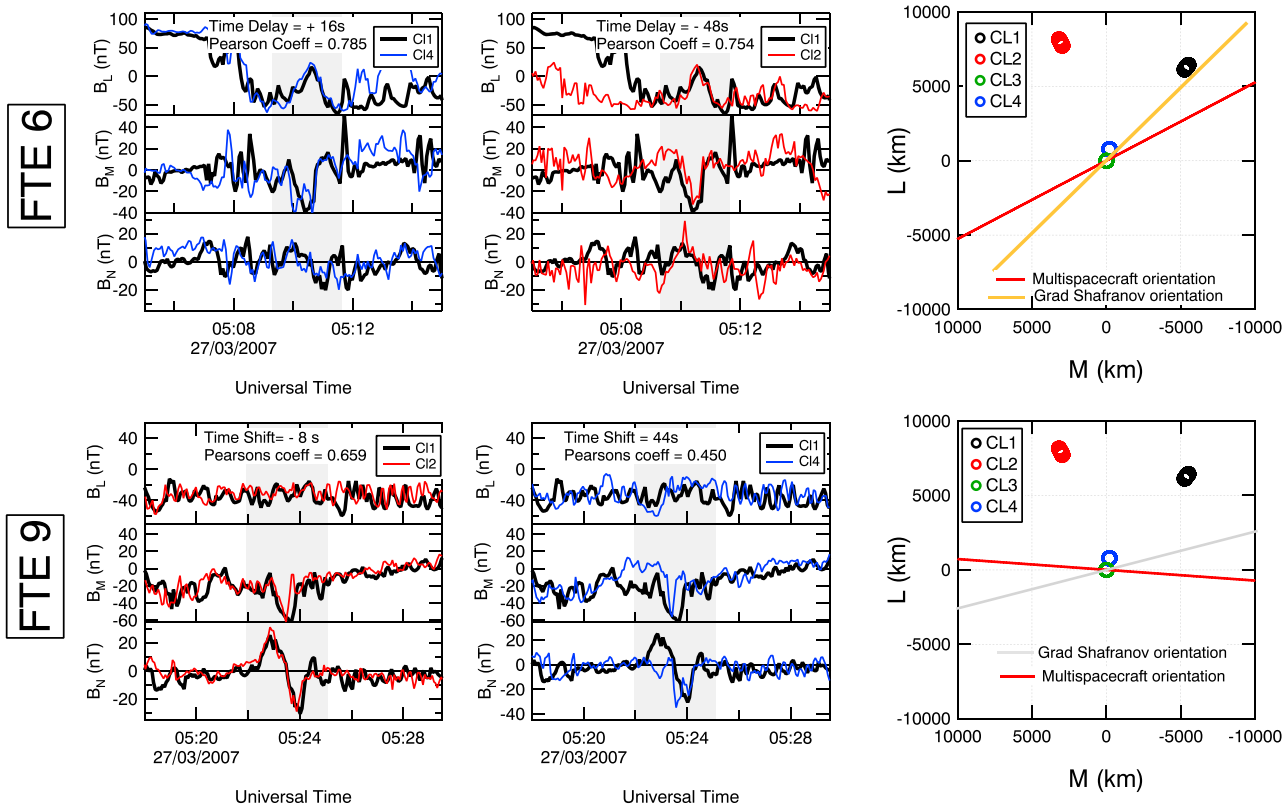

Figure 6. Magnetic field data measured by Cluster 1 together with the data measured by Cluster 2 and Cluster 4 delayed with the best time shift, on a 10 min interval around FTE 6 and FTE 9. (right column) The axial orientations obtained from multispacecraft in the magnetopause *LM* plane. As a comparison, the orientations obtained from the Grad-Shafranov analysis are also reported .

spacecraft are caused by the same FTE structure extended along the magnetopause. Caution should be taken, as *Fear et al.* [2010, 2012] have shown that there were clear differences between the FTE signatures observed at the different spacecraft, indicative that some of the FTE structures are spatially patchy on the scale of the separation of the spacecraft for this period.

Fear et al. [2010] used the multispacecraft timing method to determine the velocity and orientations of a subset of the FTEs detected by Cluster during this magnetopause crossing. Note that in contrast with the FTE identification used in the present study, which is the same as one of *Fear et al.* [2012] and it is based on the clearest FTE signatures observed by Cluster 1, *Fear et al.* [2010] selected FTEs based on their occurrence at all four spacecraft, which included some events for which the signature of B_N detected by Cluster 1 was smaller, and therefore are not included in the present analysis. In order to identify the FTEs that are observed by all four spacecraft, *Fear et al.* [2010] examined the B_N field component only. They found five FTEs that can be reliably associated at all four spacecraft, and they were all characterized by velocities directed mainly poleward, with small velocity components along *M* direction. This means that the FTE axes are all approximately aligned with the *M* direction, within $\pm 20^\circ$ (see their Table 1). Only one of the five FTEs that they argued to be observed by all four spacecraft corresponds to one of the nine FTEs examined in the present study (FTE 9).

In this study we reexamine the magnetic field data measured by the four Cluster spacecraft, to verify if any of the nine large FTEs observed by Cluster 1 and analyzed with the GS optimization can be reasonably associated with the FTEs observed by the other Cluster spacecraft. Differently from the previous analysis, in order to provide further confidence in the associations between signatures observed at the different spacecraft, we visually inspected here all three magnetic field components. We found that also FTE 6 observed by Cluster 1 can be reasonably associated with signatures at other Cluster spacecraft, given the similarity in the signatures in the B_L and B_M perturbations with high Pearson's correlation coefficient (see Figure 6), as well as FTE 9.

The best time shift was then obtained from the minimization of the deviation of Cluster 2 and Cluster 4 data with respect to Cluster 1 data, with the following procedure: the magnetic field vector measured by Cluster 2

($\vec{B}_{Cl2}$) was shifted with respect to the magnetic field vector measured by Cluster 1 ($\vec{B}_{Cl1}$) with a time shift Δt_0. For each time shift, the deviation χ^2 is evaluated in a time interval of approximately 3 min centered on each FTE, as

$$\chi^2\left(\Delta t_0\right) = \sum_i \frac{\mid \vec{B}_{Cl1}\left(t_i\right) - \vec{B}_{Cl2}\left(t_i - \Delta t_0\right) \mid}{\mid \vec{B}_{Cl1}\left(t_i\right) \mid} \tag{2}$$

The time shift that corresponds to the minimum deviation χ^2 was chosen as the best time shift. The same procedure was used to determine the best time shift for the Cluster 4 data. The data from Cluster 4 are used instead of Cluster 3 data, since Cluster 4 was closer to the magnetopause during this magnetosheath interval, and therefore, the signatures of both FTEs 6 and 9 were clearer. This method is similar to the one adopted by *Malaspina and Gosling* [2012] to match the solar wind discontinuities observed by the two Stereo spacecraft.

Figure 6 shows the magnetic field data measured by Cluster 1 together with the data measured by Cluster 2 and Cluster 4 delayed with the best time shift, in a 10 min interval around FTE 6 and FTE 9. At the top of each panel are reported the best time shifts and the average Pearson's correlation coefficients obtained as the average values of the three Pearson's coefficient relative to each *LMN* magnetic field components measured by Cluster 1 and Cluster 2 or Cluster 1 and Cluster 4 during these FTEs.

For FTE 6, we found a very good correspondence in magnetic field data measured by Cluster 1 with the data measured by both Cluster 2 and Cluster 4 and the corresponding average Pearson's correlation coefficients are high. In this case, even though Cluster 2 and Cluster 4 observe several other adjacent FTEs with similar B_N signatures, we believe that this association is reliable given the similarity of the signatures observed both in B_L and B_M components by all the three spacecraft.

In contrast, for FTE 9 we found a good correspondence only with the data measured by Cluster 2, since Cluster 4 observed an asymmetric signature in the B_N component during this FTE, which is the main reason for the lower average Pearson's correlation coefficient. These asymmetric FTEs are often observed at the magnetopause and are called FTEs with "irregular polarity" [*Rijnbeek et al.*, 1984]. In this case, however, this FTE is more isolated and the general trends of the three magnetic field components measured by Cluster 1 and Cluster 4 are quite similar both before and after the FTE. Therefore, we also consider this association reliable.

The fact that all the four Cluster spacecraft with this large separation detect these FTEs suggests that these FTEs 6 and 9 have a large axial extension along the magnetopause, and therefore, the two-dimensional geometry assumed by the GS reconstruction is a good approximation. The axial orientations obtained from multispacecraft timing for these FTEs are shown in Figure 6 (right column), where we also reported the orientations obtained from the GS analysis for comparison.

Although the orientations from multispacecraft timing show a reasonable agreement with the ones obtained from the GS optimization (the deviation is approximately 15°), the deviations of the FTE axis with respect to the orientation of the X line (along the *M* axis) are now smaller with respect to the FTE axis obtained from GS analysis. These smaller deviations of the FTE axes with respect to the X line orientation, even if there is still a nonnegligible difference between the orientations of the two FTEs (35°), are probably more consistent with the magnetopause sections of the FTEs generated by the extended X line models (single or multiple). Indeed, if we consider that reconnection could start at different times, or it could occur with different reconnection rates along the X line (X lines), the resulting FTE could be tilted with respect to the X line. A positive angle is expected on the side of the X line where reconnection starts first or where it has a higher reconnection rate (see the schematic in Figure 7).

7. Grad-Shafranov Reconstruction of FTE 9

In the final step of our analysis, we performed GS reconstruction for FTE 9, adopting the axial orientation that we obtained from multispacecraft method.

This FTE differs from the other FTEs on this crossing in several respects. It is not associated with any reconnection jet. It is also the only FTE with an axis approximately aligned with the X line orientation according to both the GS and the multispacecraft method, and it is detected by all the four Cluster spacecraft. This suggests that it is extended along the magnetopause, and therefore, it satisfies well the two-dimensional geometry

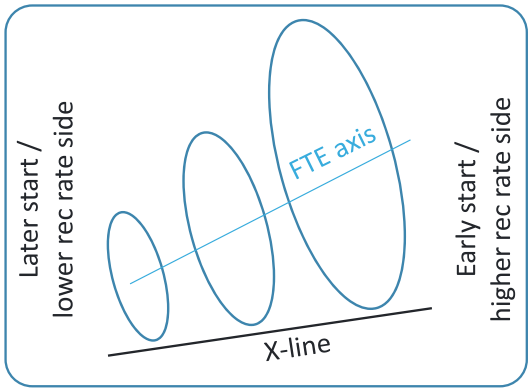

Figure 7. A scheme that illustrates an FTE with the axis tilted with respect to the X line, considering a reconnection that started at different times and/or is ongoing with different reconnection rates along the X line.

assumed by the GS analysis. Moreover, the axes determined from GS and an alternative method based on Faraday's law are remarkably consistent with each other and with the results of the Faraday's law method applied to the same signature at Cluster 2 [*Fear et al.*, 2012]. This suggests that the underlying assumptions of these methods are better satisfied for this event than the others. Furthermore, the velocity of this FTE is similar to the local magnetosheath velocity, whereas the others move at faster speeds [*Fear et al.*, 2010]; the different velocities could be consistent with FTE 9 being formed by multiple X line reconnection and the others being formed by a single X line, since modeling studies predict that multiple X line flux ropes should be embedded in the magnetosheath flow, whereas FTEs formed by single X line reconnection should move faster due to the magnetic tension force [*Ku and Sibeck*, 1998, 2000].

The result of this reconstruction obtained from the data measured by Cluster 1 is shown in Figure 8. Figure 8 (top left) shows the magnetic field components measured inside the FTE in the local reference frame used for the GS reconstruction: *Z* (along the FTE axis = dawnward) and *X* (along the velocity of the FTE = northward) are contained in the *LM* magnetopause plane, while *Y* is along magnetopause normal *N*, outward. In Figure 8

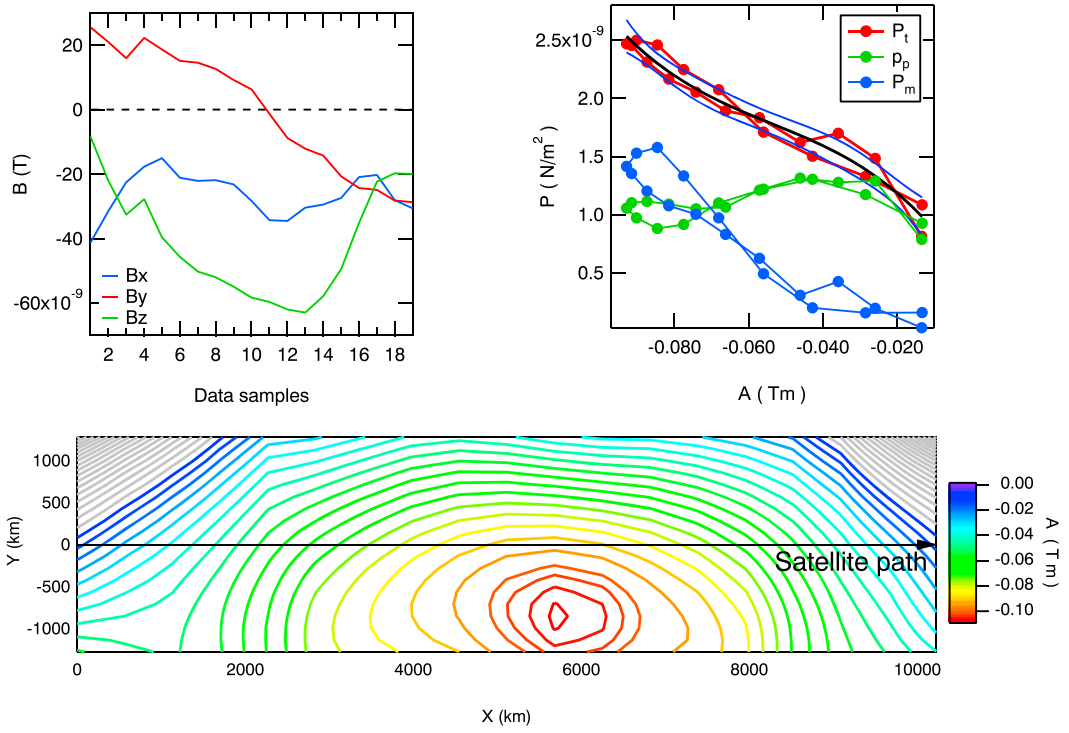

Figure 8. The result of the Grad-Shafranov reconstruction for the FTE 9 obtained from Cluster 1 data. (top left) The normal component of the velocity and the magnetic field components measured inside the FTE in the local Grad-Shafranov reference frame. (top right) The plasma pressure (p), the magnetic field pressure $\left(P_m = \frac{B_z^2}{2\mu_o}\right)$, and the total transverse pressure $\left(P_t = \left(p_p + \frac{B_z^2}{2\mu_o}\right)\right)$ as a function of the vector potential (A), and the black line is the polynomial fit of $P_t(A)$ used to perform the reconstruction. (bottom) The magnetic field map obtained from the GS reconstruction.

(top right), shown are the plasma pressure (p_p), the magnetic field pressure $\left(P_m = \frac{B_z^2}{2\mu_o}\right)$, and the total transverse pressure $\left(P_t = \left(p_p + \frac{B_z^2}{2\mu_o}\right)\right)$ measured inside the FTE as a function of the vector potential (A), and the black line is the polynomial fit of $P_t(A)$ used to perform the reconstruction. Both p_p and P_m, and consequently P_t, are single-valued functions of A, and this suggests that the FTE orientation determined from the multispacecraft timing satisfies well the GS equilibrium equation.

Figure 8 (bottom) shows the magnetic field map obtained from the GS reconstruction, following the integration scheme illustrated by *Hau and Sonnerup* [1999], in a rectangular box with a small aspect ratio ($y/x = 1/4$). This small aspect ratio ensures that the majority of the field lines in the reconstruction plane are connected with the spacecraft trajectory and therefore are obtained without extrapolation of $P_t(A)$. In this way, the reconstruction is more reliable. The field lines not magnetically connected with the spacecraft trajectory are colored in grey, while in the colored field lines the color scale represents the value of the vector potential A.

At the center of the structure, the GS reconstruction recovers several closed field lines in the reconstruction plane, and the same closed field topology can be inferred also for some of the outer field lines, even though they go outside the reconstruction plane. Cluster 1 crosses this structure slightly off the center, remaining on the magnetosheath side of the FTE, as deduced by the negative sign of the (B_x) component. At the center of this FTE the plasma pressure slightly decreases; therefore, this structure is not in a force-free equilibrium, while the axial magnetic field (B_z) increases. In three-dimensional space, this configuration would result in a flux rope with nested helical field lines. This field topology is expected in the FTEs formed by multiple X line reconnection and is typical of the topologies reproduced by GS reconstructions of FTEs [*Sonnerup et al.*, 2004; *Hasegawa et al.*, 2006].

The cross section of this FTE, more elongated in the direction parallel to the magnetopause plane (X direction) and more flat along the magnetopause normal (Y direction), could be the result of the draping of the adjacent magnetosheath and magnetospheric field lines around the FTE. The shape of FTE 9 is different from the one obtained by *Hasegawa et al.* [2010], who analyzed an FTE bounded by two converging reconnection jets and obtained a shape more elongated in the N direction. They suggested that the FTE elongation along the N direction was due to effect of the two converging jets that compressed the FTE along the L direction. Therefore, the shape obtained for FTE 9, together with the lack of adjacent reconnection jets, suggests that this FTE is observed after its formation, when reconnection at both X lines has already stopped.

Figure 9 illustrates the reconstruction of FTE 9 performed with Cluster 3 data, with the same format as Figure 8. In this reconstruction, several field lines are not magnetically connected with the spacecraft path (grey lines), and several other field lines are sampled by Cluster 3 only one time. Therefore, this reconstruction is probably less reliable and should be considered only qualitatively. In Figure 9 (top right), shown are the velocity and magnetic field components measured by Cluster 3 in a 25 min window about this FTE, using the *LMN* reference frame. The grey shading highlights the data interval used to perform the reconstruction.

In this reconstruction several open field lines are recovered, which are bent toward the magnetospheric side only in the second half of the FTE, in correspondence with the observed irregular negative (B_y) (B_N) signature. A possible explanation for this reconstruction is that this FTE is generated by a combination of single and multiple X line reconnection, and Cluster 3 is observing the more external part of this FTE, characterized by open field lines in the reconstruction plane, generated by single X line reconnection [see *Hasegawa et al.*, 2010, Figure 1c]. However, Cluster 3 does not detect any accelerated plasma flow along the L direction at the trailing edge of this FTE (i.e., any reconnection jet; see Figure 9 (top right)), which would be expected in the single X line model. Therefore, the lack of this jet is not in agreement with this hypothesis.

Another possible interpretation suggests that during the first part of the reconstruction, this magnetic structure is farther away from Cluster 3, outside the reconstruction plane along negative Y (negative N); i.e., Cluster 3 is farther from the magnetopause. Then, an outward motion of the magnetopause brings Cluster 3 closer to the center of the FTE during the second part of the reconstruction, when the negative B_y signature is observed. The behavior of the normal velocity component measured by Cluster 3 during this FTE (V_N in Figure 9 (top right)) confirms this interpretation. Indeed, even though V_N shows a bipolar signature during this FTE as expected, the positive fluctuation of V_N detected during the first part of the FTE has a much larger value and a longer duration than the negative fluctuation. This suggests that Cluster 3 observed an outward motion of the magnetopause during this FTE. The average value of V_N during this FTE (grey shading in Figure 9

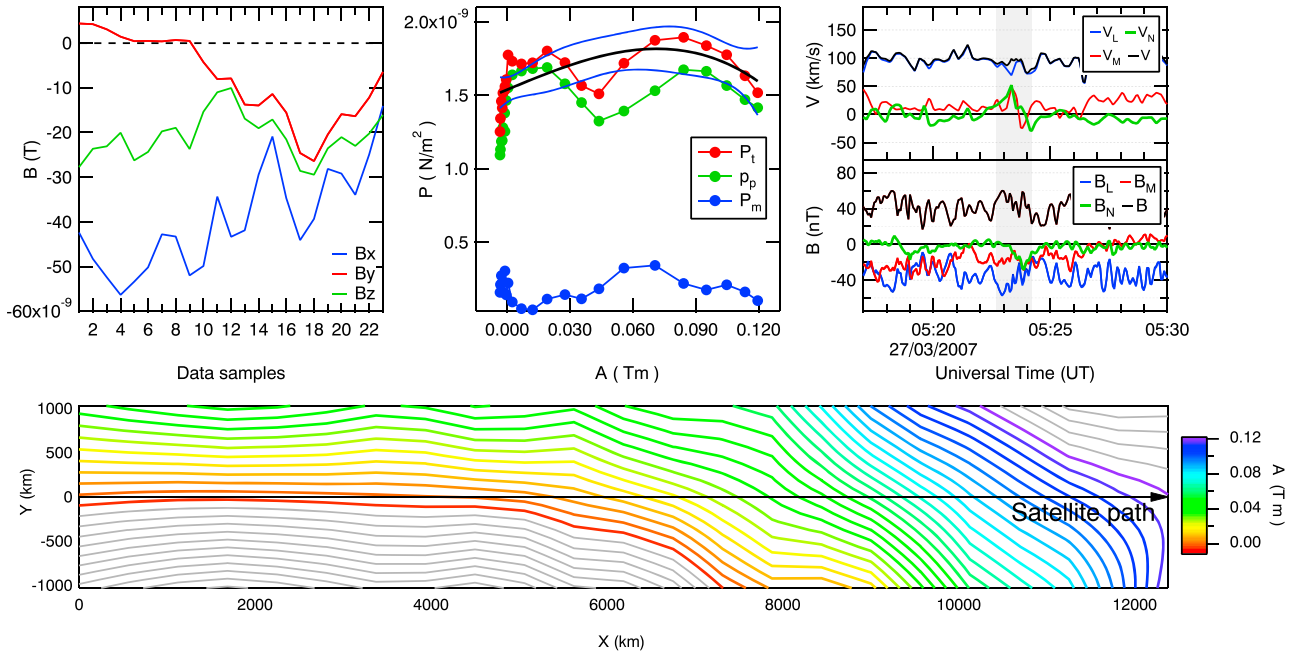

Figure 9. The result of the Grad-Shafranov reconstruction for the FTE 9 obtained from Cluster 3 data. The format is the same as Figure 8.

(top right)) is $V_N avg \sim +15$ km/s. The total displacement along the magnetopause, obtained multiplying $V_N$avg by the time duration of this FTE (96 s), is 1440 km, and it is comparable with the scale size of the FTE along the *N* direction obtained from the GS reconstruction.

8. Discussion

In this paper, we performed different analyses on several FTEs sequentially observed by Cluster 1 during the magnetopause crossing observed on 27 March 2007 near the subsolar point, in order to understand their generation mechanism.

During this magnetopause crossing, Cluster 1 detected several reconnection jets, and the relative position of these jets with respect to the FTEs provides important indication about the FTE generation. In particular, these reconnection jets, identified by means of the Walén test, are all directed northward, in the same direction as the FTE motion, and they are all located at the trailing edge of the FTEs. The use of the transition parameter allowed us to ascertain that these reconnection jets are not observed during the deepest penetration into the boundary layer but are instead propagating at the trailing edge of the FTEs. The presence of these reconnection jets is suggestive of the single X line model [*Scholer*, 1988; *Southwood et al.*, 1988], which explicitly predicts a reconnection jet moving in the same direction of the FTE propagating along its trailing edge [*Lockwood and Smith*, 1994]. Instead, in the original *Russell and Elphic* [1978] model a poleward acceleration of the plasma could be detected inside the FTE, but the velocity increase should be observed during the entire FTE and not only at its trailing edge [*Sonnerup*, 1987]. In the multiple X line model [*Lee and Fu*, 1985], two converging reconnection jets at the borders of the FTE are expected if the FTEs are observed during their formation [*Hasegawa et al.*, 2010; *Trenchi et al.*, 2011; *Øieroset et al.*, 2011; *Zhang et al.*, 2012; *Zhong et al.*, 2013; *Pu et al.*, 2013]. The lack of the southward reconnection jets at the leading edge of the FTEs could be explained possibly also in the context of multiple X line reconnection, if reconnection at the southern X line is more active and reconnection at the northern X line is not active when the FTEs are detected. In this case, a combination of single and multiple X line reconnection would be responsible for the generation of the FTEs. These two mechanisms are not necessarily mutually exclusive—it may simply be a balance of reconnection rates at two X lines [*Hasegawa et al.*, 2010]. However, no southward reconnection jet is detected during the entire magnetopause crossing and the northward reconnection jets seem to be systematically associated with the trailing edge of the FTEs. Therefore, it seems that these FTEs associated with reconnection jets at the trailing edge are generated by the single X line model.

Similar reconnection jets at the trailing edge of the FTEs were reported by *Paschmann et al.* [1982]. These authors concluded that the presence of these reconnection jets at the trailing edge of the FTEs is difficult to be reconciled with the FTE motion in the *Russell and Elphic* [1978] model and could possibly indicate the presence of some dynamical process at the trailing edge of these FTEs. However, we note that Paschmann et al.'s observations preceded the development of the single X line mechanism [*Scholer*, 1988; *Southwood et al.*, 1988].

The axial orientations determined by the GS optimization process in section 5 show considerable spread and do not seem to be compatible with the magnetopause sections of the FTEs generated by the extended X line models (single or multiple). This GS optimization is generally considered reliable when P_t is, with good approximation, a single-value function of A, such as during the FTEs in Figure 3. The presence of the reconnection jets at the trailing edge of these FTEs should not alter much the hydrostatic equilibrium assumed by the GS reconstruction, since the Walén slope evaluated inside these FTEs, in the time intervals used for the GS analysis, is generally quite small, i.e., < 0.2, and only the FTE 7 has a Walén slope of≈ 0.4 (not shown). However, it should be mentioned that while it has been proven that this method finds the correct axial orientation for flux ropes, i.e., two-dimensional structures characterized by closed field lines in the transverse plane [*Hu and Sonnerup*, 2002], as far as we know, it has never been tested with two-dimensional structures characterized by open field lines in the transverse plane, such as FTEs generated by single X line reconnection. For this reason, the orientations obtained from the GS optimization for these FTEs could be not reliable. Apart from FTE 9 (discussed below), it was only possible to verify one such axis (FTE 6) using a multispacecraft approach (section 6); the latter approach produced an axis for FTE 6 that was closer to the dawn-dusk orientation expected for the magnetopause section of the FTE expected in either the single or multiple X line model, although still tilted by $\sim 30°$ with respect to the M direction. As argued in section 6, this discrepancy can be explained if reconnection starts at different times, or occurs at different rates, along the X line (Figure 7).

FTE 9 has several features that make it different from the other FTEs observed during this crossing. It is not associated with any reconnection jet. It is the only FTE for which all the different techniques performed in this paper and in the previous studies [*Fear et al.*, 2010, 2012] consistently gave an axis approximately aligned with the X line. Moreover, it is detected by all the four Cluster spacecraft, and therefore, it is probably extended along the magnetopause, satisfying well the two-dimensional geometry assumed by the GS analysis. Furthermore, the velocity of this FTE is similar to the local magnetosheath velocity [*Fear et al.*, 2010], and this motion would be consistent with FTE 9 being formed by multiple X line reconnection [*Ku and Sibeck*, 2000]. The GS reconstruction based on Cluster 1 data (Figure 8) shows that this FTE is characterized by several closed field line loops in the reconstruction plane, which are associated with a strong axial core field. This topology produces, in three-dimensional space, a flux rope with nested helical field lines. This field topology is typical of that usually obtained from GS reconstruction of FTEs and suggests that this FTE has been formed by the multiple X line reconnection mechanism [*Lee and Fu*, 1985]. The cross section of this FTE is more elongated along the magnetopause plane than along the magnetopause normal. This feature, together with the lack of converging reconnection jets at the borders of the FTE, suggests that this FTE has been observed by Cluster 1 sometime after its formation, when reconnection at both X lines has already stopped.

Cluster 3 instead observed an asymmetric signature in the B_N component during this FTE, which is referred to as an irregular polarity [*Rijnbeek et al.*, 1984]. The reconstruction performed with Cluster 3 data (Figure 9) shows several open field lines, which are bent toward the magnetospheric side only in the second half of the FTE, in correspondence with the negative (B_N) signature. The large velocity component normal to the magnetopause measured by Cluster 3 during this FTE suggests that Cluster 3 is far from the FTE during the first half of the reconstruction, and then the outward motion of the magnetopause brings Cluster 3 closer to the FTE center, when the negative B_N signature is observed. The overall displacement of the magnetopause inferred from the average value of V_N is comparable with the scale size of the FTE along the magnetopause normal.

9. Conclusions

In summary, we suggest that different generation mechanisms could be responsible for the formation of the FTEs sequentially observed by Cluster at the subsolar magnetopause during this event. Reconnection jets moving in the same direction of the FTEs are systematically associated with the trailing edge of these FTEs.

This feature is consistent with the single X line generation mechanism. Instead, for a large FTE not associated with any reconnection jet, the GS reconstruction obtained from Cluster 1 data recovered a flux rope, indicative of multiple X line reconnection. This same FTE was observed also by Cluster 3, which detected an asymmetric signature in B_N. The behavior of the plasma velocity component normal to the magnetopause suggests that this asymmetry is related to an outward motion of the magnetopause, which brings Cluster 3 closer to the FTE center during the second half of the FTE.

Acknowledgments
This work was supported by STFC Ernest Rutherford GrantST/L002809/1, and R.C.F. was supported by STFC Ernest Rutherford Fellowship ST/K004298/2. Acknowledgments go the ISSI team "Small scale structure and transport during magnetopause magnetic reconnection: From Cluster to MMS" for the stimulating discussions. The Cluster data are publicly available via the Cluster Science Archive (http://www.cosmos.esa.int/web/csa/access).

References

Balogh, A., et al. (1207), The Cluster Magnetic Field Investigation: Overview of in-flight performance and initial results, *Annales Geophysicae*, 19.
Bogdanova, Y. V., et al. (2008), Formation of the low-latitude boundary layer and cusp under the northward IMF: Simultaneous observations by Cluster and Double Star, *J. Geophys. Res.*, *113*, A07S07, doi:10.1029/2007JA012762.
Biernat, H. K., M. F. Heyn, and V. S. Semenov (1987), Unsteady Petschek reconnection, *J. Geophys. Res.*, *92*, 3392–3396.
Daly, P. W., E. Keppler, D. J. Williams, and C. T. Russell (1981), Particle signature of magnetic flux transfer events at the magnetopause, *J. Geophys. Res.*, *86*, 1628–1632.
Fear, R. C., et al. (2005), Cluster observations of bounday layer structure and a flux transfer event near the cusp, *Ann. Geophys.*, 2605–2620.
Fear, R. C., et al. (2008), The azimuthal extent of three flux transfer events, *Ann. Geophys.*, 2353–2369.
Fear, R. C., S. E. Milan, E. A. Lucek, S. W. H. Cowley, and A. N. Fazakerley (2010), The Cluster Active Archive, *Studying the Earth's Space Plasma Environment*, 389.
Fear, R. C., S. E. Milan, and K. Oksavik (2012), Determining the axial direction of high-shear flux transfer events: Implications for models of FTE structure, *J. Geophys. Res.*, *117*, A09220, doi:10.1029/2012JA017831.
Gonzales, W. D., and F. S. Mozer (1974), A quantitative model from the potential resulting from reconnection with an arbitrary interplanetary magnetic field, *J. Geophys. Res.*, *79*, 4186–4194.
Hapgood, M. A., and D. A. Bryant (1990), Re-ordered electron data in the low-latitude boundary layer, *Geophys. Res. Lett.*, *17*, 2043–2046.
Hapgood, M. A., and D. A. Bryant (1992), Exploring the magnetospheric boundary layer, *Planet. Space Sci.*, 1431–1459.
Hapgood, M., and M. Lockwood (1995), Rapid changes in LLBL thickness, *Geophys. Res. Lett.*, *22*, 77–80.
Hasegawa, H., et al. (2006), The structure of flux transfer events recovered from Cluster data, *Ann. Geophys.*, *24*, 603–618.
Hasegawa, H., et al. (2010), Evidence for a flux transfer event generated by multiple X-line reconnection at the magnetopause, *Geophys. Res. Lett.*, *37*, L16101, doi:10.1029/2010GL044219.
Hau, L.-N., and B. U. Ö Sonnerup (1999), Two-dimensional coherent structures in the magnetopause: Recovery of static equilibria from single-spacecraft data, *J. Geophys. Res.*, *104*, 6899–6917.
Hu, Q., and B. U. Ö. Sonnerup (2001), Reconstruction of magnetic flux ropes in the solar wind, *Geophys. Res. Lett.*, *28*, 467–470.
Hu, Q., and B. U. Ö Sonnerup (2002), Reconstruction of magnetic clouds in the solar wind: Orientations and configurations, *J. Geophys. Res.*, *107*, 1142, doi:10.1029/2001JA000293.
Hu, Q., C. W. Smith, N. F. Ness, and R. M. Skoug (2004), Multiple flux rope magnetic ejecta in the solar wind, *J. Geophys. Res.*, *109*, A03102, doi:10.1029/2003JA010101.
Hudson, P. D. (1970), Discontinuities in an anisotropic plasma and their identification in the solar wind, *Planet. Space Sci.*, *18*, 1611–1622.
Kawano, H., and C. T. Russell (2005), Dual-satellite observations of the motions of flux transfer events: Statistical analysis with ISEE 1 and 2, *J. Geophys. Res.*, *110*, A07217, doi:10.1029/2004JA010821.
Ku, H. C., and D. G. Sibeck (1998), Flux transfer events produced by bursty merging at a single X line, *J. Geophys. Res.*, *103*, 14,965–14,978.
Ku, H. C., and D. G. Sibeck (2000), Flux transfer events produced by the onset of merging at multiple X lines, *J. Geophys. Res.*, *105*, 2657–2675.
Laitinen, T. V., Y. V. Khotyaintsev, M. André, A. Vaivads, and H. Rème (2010), Local influence of magnetosheath plasma beta fluctuations on magnetopause reconnection, *Ann. Geophys.*, 1053–1063.
Lee, L. C., and Z. F. Fu (1985), A theory of magnetic flux transfer at the Earth's magnetopause, *Geophys. Res. Lett.*, *12*(2), 105–108.
Lemaire, J., M. Roth, and M. J. Rycroft (1979), Control of impulsive penetration of solar wind irregularities into the magnetosphere by the interplanetary magnetic field direction, *Planet. Space Sci.*, *27*, 47–57.
Lockwood, M., and M. F. Smith (1994), Low and middle altitude cusp particle signatures for general magnetopause reconnection rate variations: 1. Theory, *J. Geophys. Res.*, *99*, 8531–8553.
Lockwood, M., S. W. H. Cowley, and T. G. Onsager (1996), Ion acceleration at both the interior and exterior Alfvén waves associated with the magnetopause reconnection site: Signatures in cusp precipitation, *J. Geophys. Res.*, *101*, 21,501–21,515.
Lockwood, M., and M. A. Hapgood (1997), How the magnetopause transition parameter works, *Geophys. Res. Lett.*, *24*, 373–376.
Lockwood, M., and M. A. Hapgood (1998), On the cause of a magnetospheric flux transfer event, *J. Geophys. Res.*, *103*, 26,453–26,478.
Lui, A. T. Y., et al. (2008), Reconstruction of a magnetic flux rope from THEMIS observations, *Geophys. Res. Lett.*, *35*, L17S05, doi:10.1029/2007GL032933.
Malaspina, D. M., and J. T. Gosling (2012), Two spacecraft observations of magnetic discontinuities in the solar wind with STEREO, *J. Geophys. Res.*, *117*, A04109, doi:10.1029/2011JA017375.
Mitchell, D. G., F. Kutchko, D. J. Williams, T. E. Eastman, and L. A. Frank (1987), An extended study of the low-latitude boundary layer on the dawn and dusk flanks of the magnetosphere, *J. Geophys. Res.*, *92*, 7394–7404.
Möstl, C., et al. (2009), The structure of an earthward propagating magnetic flux rope early in its evolution: Comparison of methods, *Ann. Geophys.*, *27*, 2215–2224.
Němeček, Z., et al. (2015), Analysis of temperature versus density plots and their relation to the LLBL formation under southward and northward IMF orientations, *J. Geophys. Res. Space Physics*, *120*, 3475–3488, doi:10.1002/2014JA020308.
Øieroset, M., et al. (2011), Direct evidence for a three-dimensional magnetic flux rope flanked by two active magnetic reconnection X lines at Earth's magnetopause, *Phys. Rev. Lett.*, *107*, 165007.
Paschmann, G., et al. (1982), Plasma and magnetic field characteristics of magnetic flux transfer events, *J. Geophys. Res.*, *87*, 2159–2168.
Paschmann, G., W. Baumjohann, N. Sckopke, I. Papamastorakis, C. W. Carlson, B. U. Ö. Sonnerup, and H. Lühr (1986), The magnetopause for large magnetic shear—AMPTE/IRM observations, *J. Geophys. Res.*, *91*, 11,099–11,115.
Petschek, H. E. (1964), *Magnetic Field Annihilation*, vol. 50, 425 pp., NASA Special Publication, Washington, D. C.
Phan, T. D., G. Paschmann, and B. U. Ö. Sonnerup (1996), Low-latitude dayside magnetopause and boundary layer for high magnetic shear: 2. Occurrence of magnetic reconnection, *J. Geophys. Res.*, *101*, 7817–7828.

Pu, Z. Y., et al. (2013), Magnetic topologies of an in vivo FTE observed by Double Star/TC-1 at Earth's magnetopause, *Geophys. Res. Lett.*, *40*, 3502–3506, doi:10.1002/grl.50714.
Raeder, J. (2006), Flux transfer events: 1. Generation mechanism for strong southward IMF, *Ann. Geophys.*, *24*, 381–392.
Rème, H., et al. (2001), First multispacecraft ion measurements in and near the Earth's magnetosphere with the identical Cluster Ion Spectrometry (CIS) experiment, *Ann. Geophys.*, *19*, 1303–1354.
Rijnbeek, R. P., S. W. H. Cowley, D. J. Southwood, and C. T. Russell (1984), A survey of dayside flux transfer events observed by ISEE 1 and 2 magnetometers, *J. Geophys. Res.*, *89*, 786–800.
Russell, C. T., and R. C. Elphic (1978), Initial ISEE magnetometer results—Magnetopause observations, *Space Sci. Rev.*, *22*, 681–715, doi:10.1007/BF00212619.
Sanny, J., D. G. Sibeck, C. C. Venturini, and C. T. Russell (1996), A statistical study of transient events in the outer dayside magnetosphere, *J. Geophys. Res.*, *101*, 4939–4952.
Sibeck, D. G., W. Baumjohann, R. C. Elphic, D. H. Fairfield, and J. F. Fennell (1989), The magnetospheric response to 8-minute period strong-amplitude upstream pressure variations, *J. Geophys. Res.*, *94*, 2505–2519.
Scholer, M. (1988), Magnetic flux transfer at the magnetopause based on single X line bursty reconnection, *Geophys. Res. Lett.*, *15*, 291–294, doi:10.1029/GL015i004p00291.
Song, P., C. T. Russell, R. C. Elphic, J. T. Gosling, and C. A. Cattell (1990), Structure and properties of the subsolar magnetopause for northward IMF—ISEE observations, *J. Geophys. Res.*, *95*, 6375–6387.
Sonnerup, B. U. Ö. (1974), The reconnecting magnetosphere, in *Magnetospheric Physics*, edited by B. M. McCormac, p. 23, D. Reidel, Dordrecht-Holland.
Sonnerup, B. U. O. (1987), On the stress balance in flux transfer events, *J. Geophys. Res.*, *92*, 8613–8620.
Sonnerup, B. U. Ö., and M. Guo (1996), Magnetopause transects, *Geophys. Res. Lett.*, *23*, 3679–3682.
Sonnerup, B. U. Ö., H. Hasegawa, and G. Paschmann (2004), Anatomy of a flux transfer event seen by Cluster, *Geophys. Res. Lett.*, *31*, L11803, doi:10.1029/2004GL020134.
Sonnerup, B. U. Ä., H. Hasegawa, W.-L. Teh, and L.-N. Hau (2006), Grad-Shafranov reconstruction: An overview, *J. Geophys. Res.*, *111*, A09204, doi:10.1029/2006JA011717.
Southwood, D. J., C. J. Farrugia, and M. A. Saunders (1988), What are flux transfer events?, *Planet. Space Sci.*, *36*, 503–508, doi:10.1016/0032-0633(88)90109-2.
Trenchi, L., et al. (2008), Occurrence of reconnection jets at the dayside magnetopause: Double Star observations, *J. Geophys. Res.*, *113*, A07S10, doi:10.1029/2007JA012774.
Trenchi, L., M. F. Marcucci, H. Rème, C. M. Carr, and J. B. Cao (2011), TC-1 observations of a flux rope: Generation by multiple X-line reconnection, *J. Geophys. Res.*, *116*, A05202, doi:10.1029/2010JA015986.
Trenchi, L., R. Bruno, R. D'Amicis, M. F. Marcucci, and D. Telloni (2013), Observations of IMF coherent structures and their relationship to SEP dropout events, *Ann. Geophys.*, 1333–1341.
Trenchi, L., M. F. Marcucci, and R. C. Fear (2015), The effect of diamagnetic drift on motion of the dayside magnetopause reconnection line, *Geophys. Res. Lett.*, *42*, 6129–6136, doi:10.1002/2015GL065213.
Varsani, A., et al. (2014), Cluster observations of the substructure of a flux transfer event: Analysis of high-time-resolution particle data, *Ann. Geophys.*, *32*, 1093.
Zhang, H., et al. (2012), Generation and properties of in vivo flux transfer events, *J. Geophys. Res.*, *117*, A05224, doi:10.1029/2011JA017166.
Zhong, J., et al. (2013), Three-dimensional magnetic flux rope structure formed by multiple sequential X-line reconnection at the magnetopause, *J. Geophys. Res. Space Physics*, *118*, 1904–1911, doi:10.1002/jgra.50281.